Spatiotemporal bifurcations of a parametrically excited solitary wave

Likun Zhang,* Xinlong Wang,† and Zhiyong Tao‡
Institute of Acoustics, Nanjing University, Nanjing 210093, China
(Received 14 August 2006; revised manuscript received 7 December 2006; published 6 March 2007)

The bifurcation behaviors of a parametrically excited solitary wave are investigated via Faraday's water tank experiment. It is observed that, as the driving frequency f_d is decreased or/and the driving amplitude A_d is increased, the standing (but vertically oscillatory) solitary wave becomes modulationally unstable, leading to the temporal modulation of the vertical oscillation and the emergence of very low subharomic components on the frequency spectrum. Further lowering f_d or/and increasing A_d will cause the modulational oscillation unstable and then, the peak of the solitary wave becomes rocking along the trough in the longitudinal direction. These bifurcations also give rise to the emission of continuous waves resulting in complex wave patterns and complicated fluctuations, especially for the quite low f_d and large A_d. A possible route from solitary waves to chaos via bifurcations and mode competitions is therefore suggested on the basis of these observations.

DOI: 10.1103/PhysRevE.75.036602 PACS number(s): 05.45.Yv, 43.25.+y, 47.20.Ky, 47.35.−i

Solitons (or solitary waves) and chaos seem to be the opposite extremities in the rich spectrum of nonlinear phenomena. On one side, solitons appear as temporally regular and spatially coherent localized wave objects. On the other side, chaos exhibits stochasticity in deterministic nonlinear systems, or even turbulent behaviors in spatially extended systems. Partly owing to the fundamental differences, the studies of the two classes of nonlinear phenomena have usually been pursued along quite different approaches. However, there have been found numerous examples [1–3] in real physical systems where both solitonic and chaotic phenomena can be supported by changing physical conditions or varying system parameters. It is now known that solitons may exhibit bifurcation and even chaotic behaviors by introducing additional physical effects (e.g., dissipation and driving) into integrable systems, such as those found in the perturbed Korteweg de Vries (KdV) [4,5], the damped driven sine-Gordon [6–8], and the driven nonlinear Schrödinger (NLS) [9–11] systems. Thus there arises the problem of how to establish the link between the seemingly utterly different nonlinear phenomena, in particular, the routes of dynamical transition from one to the other [1,7,10–14] in the spatially extended systems. This work is an attempt to step towards the general understanding of the nonlinear dynamics of solitons.

We explore the problem by experimentally investigating the dynamical behaviors of the parametrically excited soliton [3,15] which can be easily realized and controlled in Faraday's water wave resonator. Not only in the Faraday experiment but also in a variety of physical systems [14] have the parametrically resonant wave phenomena been found. By assuming weak damping and driving and incorporating cubic nonlinearity, parametrically excited waves can usually be described by the simplified model, i.e., the parametrically driven nonlinear Schrödinger (PDNLS) equation

$$i(\phi_\tau + \alpha\phi) + \phi_{XX} + \beta\phi + 2|\phi|^2\phi + \gamma\phi^* = 0, \tag{1}$$

where the asterisk "*" denotes the complex conjugate, β is the frequency detuning or normalized driving frequency, and γ is the dimensionless driving strength. This equation admits a standing soliton [16] which can be observed in the oscillating water trough [15].

Early experimental observation [17] has already demonstrated that the standing soliton can be sustainable only if the driving parameters, (β, γ) in Eq. (1), fall into what was called the "stability region." For details, readers are referred to our previous work [17]. Theoretical analysis of Eq. (1) verified the existence of the parameter region [18,19]. Further investigations provided the evidence for the bifurcation and the possible onset of chaos [20–22]. The numerical simulations of Eq. (1) also showed the possibility of the period-doubling and quasiperiodic transitions to chaos in the neighborhood of the stable region [14,23]. However, the problem still remains unclear or ambiguous as to the general scenario of the bifurcation from the orderly standing localized wave state to complex motions, and a systematic experimental survey is required to supply a clear physical picture about the nonlinear dynamics of the solitons, especially the spatiotemporal bifurcation behaviors of the solitary waves and the possible transition to chaos.

We perform the experiment in a vertically vibrating long trough of length $L=20$ cm and width $W=2.5$ cm, filled with static water of depth $d=2.0$ cm. To reduce the surface tension effect, a small amount of saponin is added to the pure water. In what follows we always assume that the reference frame is fixed to the vibrating trough and is so set that the fluid at rest occupies the rectangular region $-L/2<x<L/2$, $0<y<W$, and $-d<z<0$. The vertical vibration of the container takes the simple harmonic form

$$z_0 = A_d \cos(4\pi f_d t). \tag{2}$$

The driving frequency, $f_d=\omega_d/(2\pi)$, and amplitude A_d of the vibration relate to the dimensionless ones, β and γ in Eq. (1), as [3]

*Electronic address: zhanglikun@nju.org.cn
†Corresponding author. Electronic address: xlwang@nju.edu.cn
‡Electronic address: zytao@nju.edu.cn

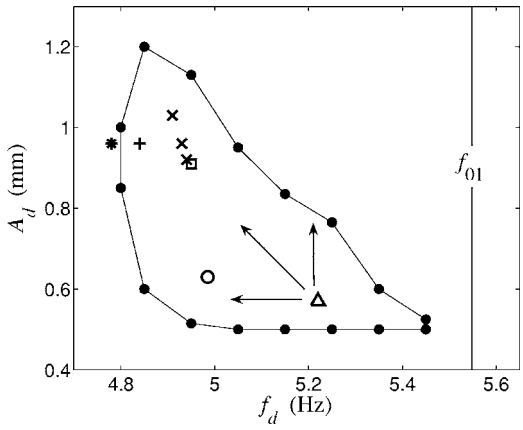

FIG. 1. Stablility region (inside the closed curve consisting of the line-connected bold dots) in the driving parameter (f_d,A_d) space. The bold dots are the measured data of the boundary points of the stability region.

$$\beta = \frac{\omega_d^2 - \omega_{01}^2}{2\omega_{01}^2}, \quad \gamma = \frac{4\omega_d^2 A_d}{g}, \tag{3}$$

respectively, with ω_{01} being the linear angular eigenfrequency of the first transverse mode of the water resonator, and g the gravitational acceleration. For this configuration, the stability region of the soliton on the (f_d, A_d) plane was given in [17], and replotted in Fig. 1, where the vertical line labeled by f_{01} denotes the linear cutoff frequency f_{01} of the first transverse surface-wave mode (0,1).

Taking (f_d, A_d) as the bifurcation parameters and varying them on the (f_d, A_d) plane as indicated by the arrows in Fig. 1, we can investigate the dynamics of the solitons. The surface response is detected by a pair of (closely separated) parallel electrodes vertically dipping into water.

When the driving frequency f_d is close to f_{01} and the driving amplitude A_d is quite small, i.e., (f_d, A_d) is located on the lower right part of the stability region such as the "△" point in Fig. 1, the created soliton appears as a standing localized wave envelope along the trough, sloshing transversely exactly at Faraday's frequency f_d. Hence the fast Fourier transform (FFT) spectrum of the surface response, namely, at the peak of the wave envelope near one side wall of the trough, consists of the fundamental f_d component and its superharmonics as well. As already reported [21], by reducing f_d and (or) increasing A_d, as indicated by the arrowed lines in Fig. 1, there occurs the slow modulation of the solitary-wave oscillation, as is shown in Fig. 2(a). As a result, a very low subharmonic component f_t emerges in the spectrum of the surface response, as is shown in Fig. 2(b). The subharmonic frequency f_t being read from Fig. 2(b) is about 0.295 Hz, which is much lower than the fundamental one, f_d=4.985 Hz, the Faraday frequency. Even so, the localized wave still holds a perfect solitary shape. Since the surface response along the trough is synchronized (in phase), we call the phenomenon the *temporal bifurcation*. It is recognized as the Hopf bifurcation due to the modulational instability (MI). The modulation is found to vary with the driving parameters (f_d, A_d). As (f_d, A_d) moves to the upper left on

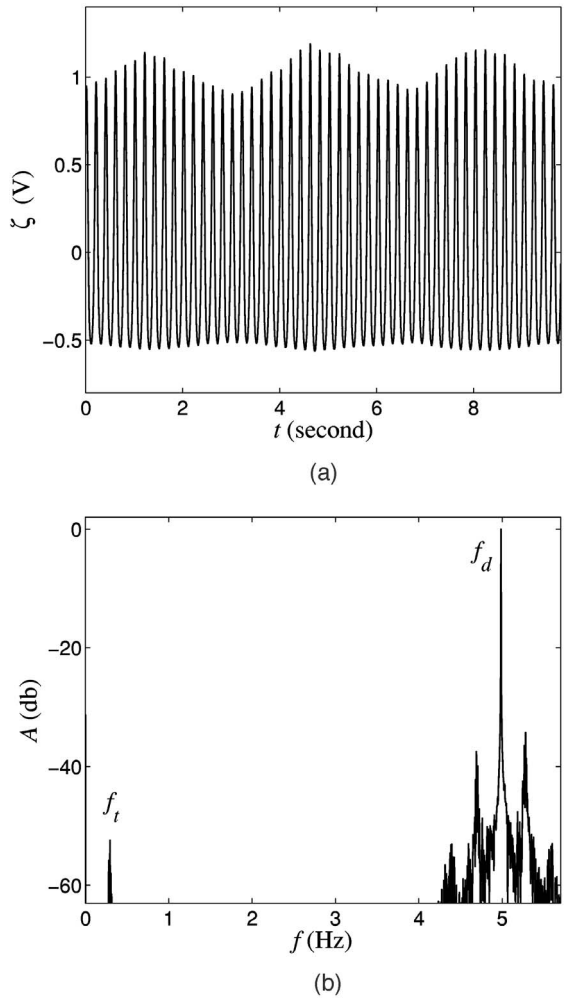

FIG. 2. The temporal modulation of soliton: (a) the time response ζ detected by the electrodes and (b) its power spectrum. The response signal is detected at the peak of a solitary-wave envelope and near one width side wall of the trough for f_d=4.985 Hz and A_d=0.630 mm, i.e., the parameter point "○" in Fig. 1.

the (f_d, A_d) plane, i.e., f_d is decreased or/and A_d is increased, the amplitude of the spectral line increases, while the subharmonic frequency f_t increases as f_d or/and A_d is increased (we will elaborate the dependence of f_t on the driving parameters with more details later and in Fig. 6).

When f_d is lowered or (and) A_d is increased to certain threshold values, we observe the breaking of the spatial sym-

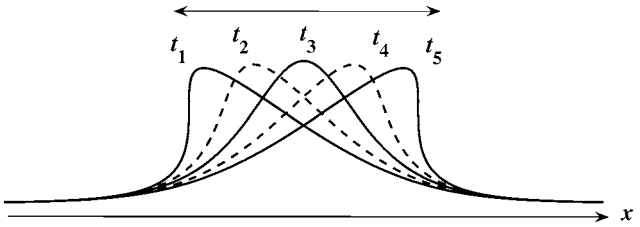

FIG. 3. Schematic plot of the peak rocking at different times in a wobbling period $(t_1 \to t_5 \to t_1)$, that is, the solitary-wave peak turns right $(t_1 \to t_2 \to t_3 \to t_4 \to t_5)$ and left $(t_5 \to t_4 \to t_3 \to t_2 \to t_1)$ alternatively in the x direction.

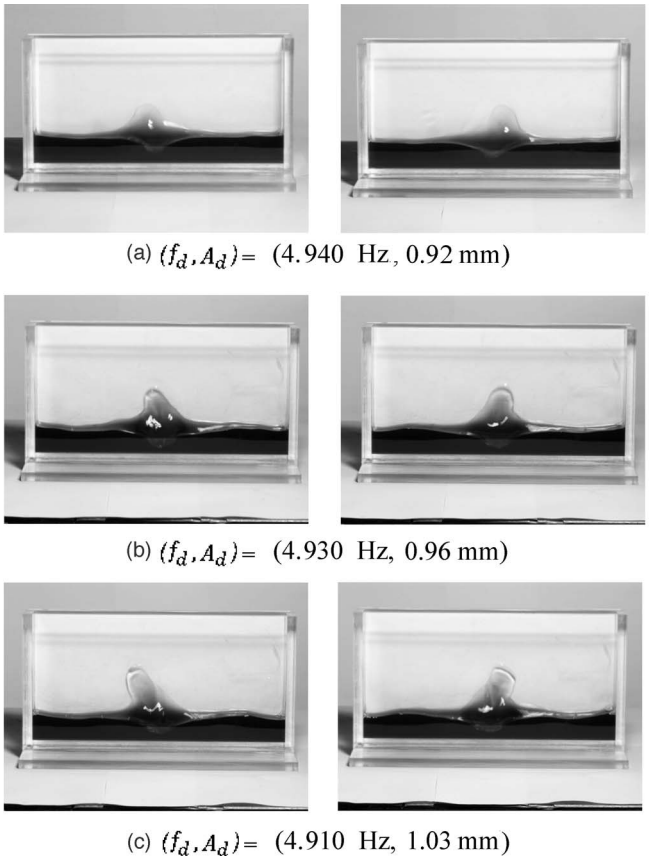

FIG. 4. The photos of the wave peak turning left and right, for (f_d, A_d) corresponding to the three "×" points in Fig. 1, respectively.

metry of the localized wave structure, and the solitary-wave begins rocking or "shaking its head" along the trough, that is, the solitary-wave peak turns left and right alternatively in the x direction. Figure 3 describes the rocking phenomenon schematically, and Fig. 4 presents the pictures taken when the wave peak turns left and right, respectively, for the three sets of driving parameters, (f_d, A_d), labeled as the "×" points in Fig. 1. The symmetry breaking changes the spatial sym-

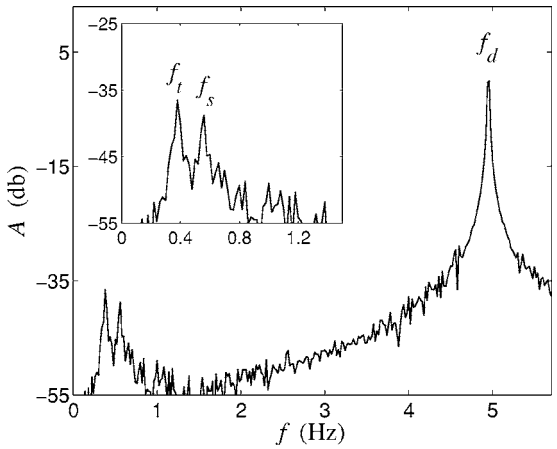

FIG. 5. The FFT power spectrum of the rocking soliton for f_d=4.950 Hz and A_d=0.92 mm. The inset is the magnified portion in the lower frequency range from 0 to 1.6 Hz.

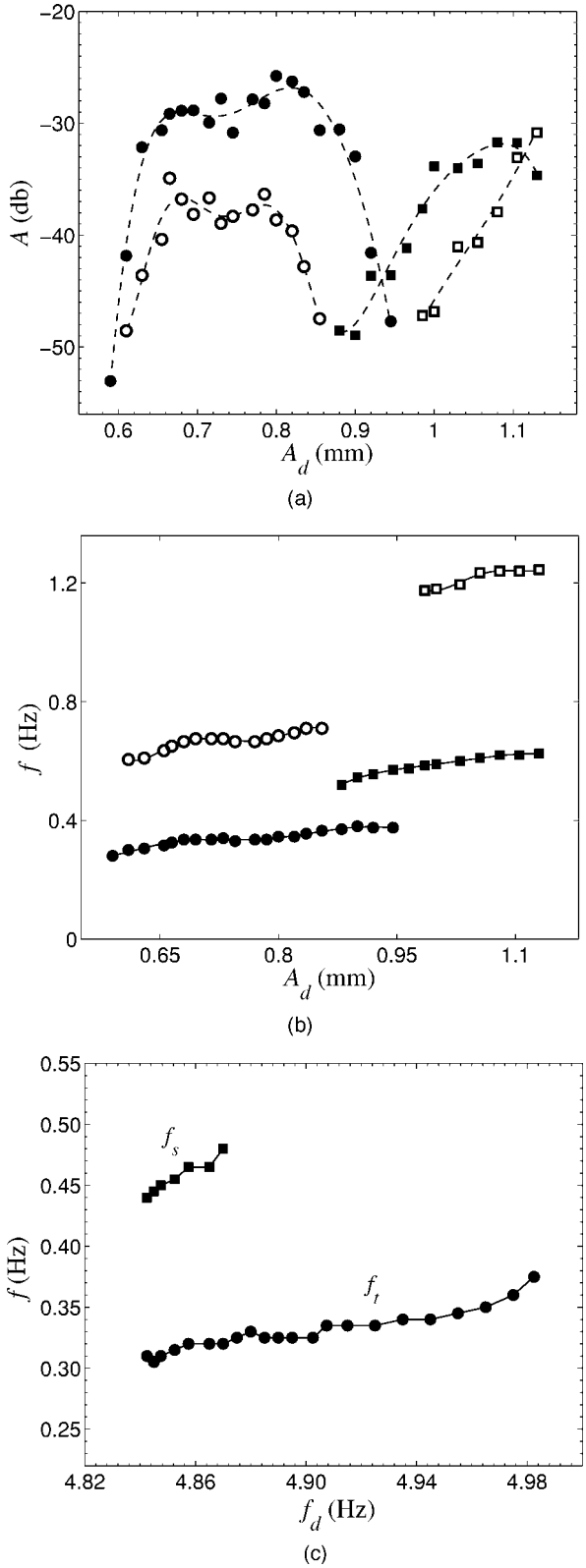

FIG. 6. The subharmonic amplitude A (a) and frequency (b) vs the forcing amplitude A_d at the fixed f_d=4.950 Hz, and (c) is the subharmonic frequency vs the forcing frequency f_d at the fixed A_d=0.80 mm. The filled and empty circles are the experimental data for the f_t and $2f_t$, and the filled and empty squares are those for f_s and $2f_s$.

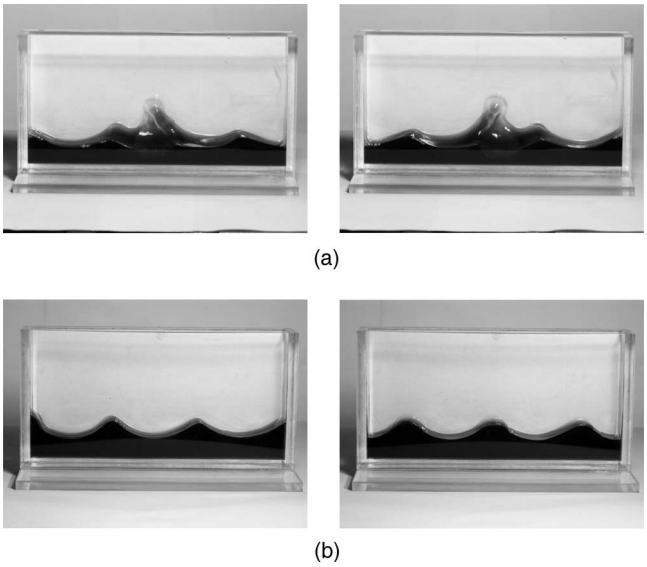

FIG. 7. (a) Emission of continuous wave tails when the solitary wave is in strong rocking state (f_d=4.840 Hz and A_d=0.96 mm, i.e., the "+" point in Fig. 1). (b) The excitation of longitudinal modes as the solitary waves losing stability (f_d=4.790 Hz and A_d=0.96 mm, i.e., the "*" point in Fig. 1). (The left and right pictures in (a) and (b) are taken at different times).

metry of the solitary wave, leading to the *spatial bifurcation* that is distinct from the temporal (Hopf) bifurcation described above. The rocking frequency, denoted by f_s, is measured to be much lower than the Faraday frequency f_d, but slightly larger than f_t. As a result, in the FFT spectrum, there emerges another subharmonic component at f_s, in addition to the MI-induced subharmonic f_t. Figure 5 shows the spectral structure for f_d=4.950 Hz and A_d=0.92 mm (i.e., the "□" parameter point in Fig. 1) at which the peak rocking just initiates. From the figure, we read that f_s=0.570 Hz and f_t =0.375 Hz. We find that the coexistence of both f_t and f_s subharmonic components does not last as (f_d, A_d) further moves to upper left on the (f_d, A_d) plane. With the continuing lowering of f_d or/and increasing of A_d, the level of the f_t spectral line declines rapidly, and at the same time, the peak rocking becomes so strong that the solitary-wave form becomes multiple-valued when the peak turns either left or right, as already indicated in Fig. 4(b). At certain (f_d, A_d), the MI-induced subharmonic f_t is completely depressed, and the f_s component dominates the low-frequency motions.

The variations of the subharmonic spectral components with the driving parameters are measured and plotted in Fig. 6. Figure 6(a) shows how the heights of the spectral lines, f_t and f_s (and their superharmonics), depend on the driving amplitude A_d at the fixed frequency f_d=4.950 Hz. The filled and empty circles in the figure are the experimental data, respectively, for f_t and $2f_t$, and the filled and empty squares are those for f_s and $2f_s$. It can be seen that the strength of the temporal modulation (the f_t component) grows rapidly for A_d<0.70 mm, and then almost keeps constant for 0.7<A_d <0.8 mm. For A_d>0.8 mm, the amplitude of the f_t line declines rapidly, signaling the onset of the spatial bifurcation and the transition to the rocking motion. At $A_d \approx 0.9$ mm, the peak rocking becomes quite visible, and the amplitude of the

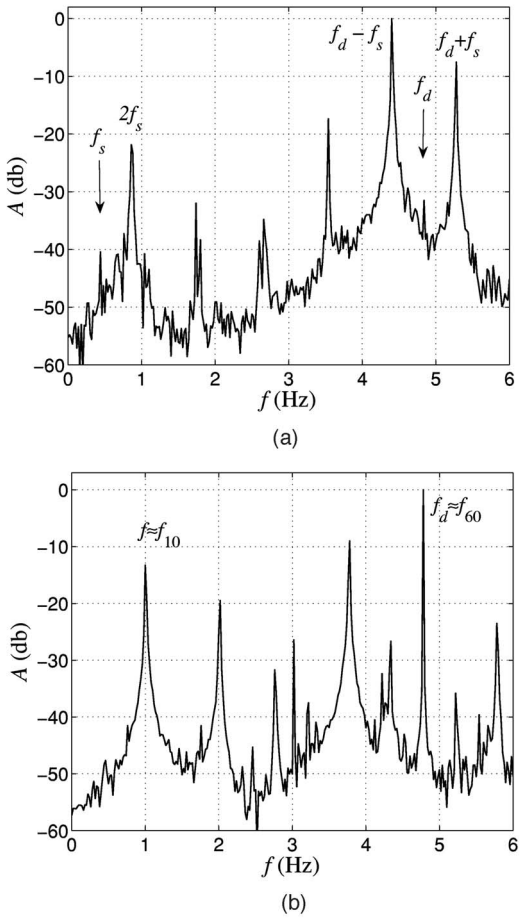

FIG. 8. The FFT power spectrum of the surface response detected at in the middle of one end wall (x=10 cm, y=1.25 cm), where f_s=0.44 Hz. The driving parameters are the same as in Figs. 7(a) and 7(b), respectively.

f_s line grows rapidly for A_d greater than 0.9 mm. In Fig. 6(c), the values of both f_t and f_s subharmonics are plotted against the driving frequency f_d at the fixed A_d=0.80 mm. It seems from the measured data that both subharmonic frequencies are continuous functions of A_d and f_d, implying that both f_t and f_s are incommeasurable to f_d and the corresponding wave motions are quasiperiodic.

We also observe that even the temporal modulation can cause the emission of continuous waves of very small amplitude from the localized site, forming the symmetrical wave tails on both sides of the solitary wave. In the rocking state, the tails of continuous waves are remarkably enhanced and unlike the temporal modulation, they become asymmetric on both sides. The traveling continuous waves will reflect on both ends of the trough, resulting in a much more complex wave pattern. At a very low f_d and large A_d, the rocking motion becomes so strong that the amplitude of the continuous waves is comparable to that of the solitary wave, and the solitary wave seems almost submerged by the continuous waves, as is shown in Fig. 7(a).

To better understand the wave dynamics, we now detect the surface response of continuous waves by placing the measuring electrodes in the middle of one of the end walls,

namely, $(x,y)=(L/2,W/2)=(10,1.25)$ cm, which is one of the wave nodes of the $(0,1)$ transverse mode. Undoubtedly, at this position the main spectral component at $f=f_d$ should vanish. We find that the $2f_s$ spectral component becomes much stronger than the f_s component at the measuring position, and it grows as the rocking motion becomes strong by lowering f_d and increasing A_d. In the strong rocking state, the fast fourier transform (FFT) power spectrum, as is shown in Fig. 8(a), has an enhanced thick noise background, and this means the complicated temporal fluctuations.

Such a complicated and composite wave motion will finally lose its stability and the solitary wave is completely destroyed as soon as (f_d, A_d) moves out of the stability region on the (f_d, A_d) plane by lowering f_d or (and) increasing A_d. Then the longitudinal surface-wave modes are resonantly excited, as is shown in Fig. 7(b), and the dominant mode is the $(6,0)$ mode for its linear natural frequency,

$$f_{60}=\frac{1}{2\pi}\sqrt{g\frac{6\pi}{L}\tanh\frac{6\pi d}{L}}\approx 4.727\ \text{Hz}, \tag{4}$$

approximates the driving frequency $f_d=4.790$ Hz. Comparing Fig. 7(a) with Fig. 7(b), the longitudinal distribution of the $(6,0)$ mode's antinodes and nodes almost coincide with that of the continuous waves in the rocking state. This uniformity implies that the rocking motion leads to the resonant excitation of the longitudinal surface-wave mode whose linear natural frequency is close to f_d. Besides, the FFT spectrum of the longitudinal modes, as is shown in Fig. 8(b), is rich in subharmonics. The lowerest one is the peak located at $f\approx 1.0$ Hz. It approximates the linear eigenfrequency f_{10} of the first longitudinal mode $(1,0)$, $f_{10}\approx 1.089$ Hz, showing the resonant excitation of the $(1,0)$ mode, a slowly sloshing motion along the trough. Therefore the longitudinal wave is mainly composed of the $(1,0)$ and $(6,0)$ modes. As is seen in Fig. 8(b), it also exhibits a certain complexity in dynamics due to the multimode interactions and competitions.

In an earlier investigation [22], the rocking motion was once observed in a double-soliton state (which was named "top oscillation" there). It was attributed to the competition between the (0,1) mode solitary waves and some longitudinal modes. However, according to the present experiment, there is no evidence for the longitudinal modes being excited while the solitary wave first becomes rocking. On the contrary, it is the rocking motion of the soliton that irritates the longitudinal modes including the $(1,0)$ mode and then gives rise to the resonant excitation of longitudinal waves. Therefore we ascertain that the spatial bifurcation, together with the temporal (Hopf) bifurcation, should be the dynamic behavior intrinsic to the soliton.

The resonant excitation of the longitudinal waves prevents us from further exploring the complex dynamics of the solitary wave in experiment, and we are not sure whether the soliton-bearing transverse wave motion would finally exhibit spatiotemporal chaos or not. However, it is quite certain that, with the decrease of f_d or/and the increase of A_d, the solitary-wave motion undergoes a dynamic process from simplicity to complexity, i.e., at first the oscillatory soliton loses its stability and becomes slowly modulated (the temporal bifurcation), then goes through the rocking motion (the spatial bifurcation), and finally, exhibits a complex wave pattern by the enhancement of continuous waves. We therefore conjecture that this might be the particular route from solitary waves to chaos via the internal bifurcations, which was not observed in the previous studies.

In conclusion, we have investigated the spatiotemporal bifurcation behaviors of solitary waves based on Faraday's experiment. In the experiment, the dynamics of the standing solitary wave is observed by varying the bifurcation parameters, i.e., the driving parameters (f_d,A_d), from the lower right to the upper left on the (f_d,A_d) plane. Based on the PDNLS equation (1), the temporal bifurcation induced by modulational instability was studied, both numerically and analytically, by several authors [11,14,23], and their results are in qualitative agreement with our experimental observation. The rocking phenomenon of a solitary wave is recognized as the spatial bifurcation also intrinsic to the soliton but completely distinct from the temporal bifurcation. In the present work we have made the attempt to numerically simulate the interesting phenomenon with Eq. (1), but no encouraging result has been achieved so far, and it seems questionable to numerically reproduce this interesting phenomenon from such an oversimplified mathematical model derived under the assumptions of weak nonlinearity, weak dispersion, and linear damping [16]. We believe that a more advanced mathematical model that incorporates higher-order physical effects (such as higher order nonlinearity than the cubic one) is needed to fully describe the highly nonlinear phenomenon. This interesting work is underway.

The project was supported by the National Science Foundation of China under Grants No. 19925414 and No. 10474045, and the Special Funds for Doctor's Degree Project of China under Grant No. 20050284018.

[1] D. Hennig, Phys. Rev. E **59**, 1637 (1999).
[2] D. V. Skryabin, Phys. Rev. E **60**, R3508 (1999).
[3] X. Wang and R. Wei, Phys. Rev. Lett. **78**, 2744 (1997).
[4] B. Birnir, Physica D **19**, 238 (1986).
[5] M. A. Allen and G. Rowlands, J. Plasma Phys. **64**, 475 (2000).
[6] A. R. Bishop and P. S. Lomdahl, Physica D **18**, 54 (1986).
[7] R. Grauer and Y. S. Kivshar, Phys. Rev. E **48**, 4791 (1993).
[8] N. Gronbech-Jensen, Y. S. Kivshar and M. R. SamuelsonPhys. Rev. B **47**, 5013 (1993).
[9] M. Taki *et al.*, Physica D **40**, 65 (1989).
[10] I. V. Barashenkov and Y. S. Smirnov, Phys. Rev. E **54**, 5707 (1996).
[11] N. V. Alexeeva *et al.*, Nonlinearity **12**, 103 (1999).
[12] F. K. Abdullaev, Phys. Rep. **179**, 1 (1989).
[13] Y. S. Kivshar and B. Malomed, Rev. Mod. Phys. **61**, 763 (1989).
[14] M. Bondila, I. V. Barashenkov, and M. M. Bogdan, Physica D **87**, 314 (1995).
[15] J. Wu, R. Keolian, and I. Rudnick Phys. Rev. Lett. **52**, 1421 (1984).

[16] J. W. Miles, J. Fluid Mech. **148**, 451 (1984).
[17] X. L. Wang and R. J. Wei, Phys. Lett. A **192**, 1 (1994).
[18] E. W. Laedke and K. H. Spatschek, J. Fluid Mech. **223**, 589 (1991).
[19] I. V. Barashenkov, M. M. Bogdan, and V. I. Korobov, Europhys. Lett. **15**, 13 (1991).
[20] R. J. Wei *et al.*, J. Acoust. Soc. Am. **88**, 469 (1990).
[21] X. L. Wang, R. J. Wei, and B. R. Wang, J. Nanjing Univ. Sci. Technol. (Natural Sci. Edition) **31** (Acoustical Issue), 13 (1995).
[22] J. Tu *et al.*, Phys. Lett. A **304**, 79 (2002).
[23] H. Friedel, E. W. Laedke, and K. H. Spatschek, J. Fluid Mech. **284**, 341 (1995).